

Supramolecular polymorphism of DNA in non-cationic L_α lipid phases

E.R. Teixeira da Silva^{1,a}, E. Andreoli de Oliveira², A. Février¹, F. Nallet¹, and L. Navailles^{1,b}

¹ Université de Bordeaux, Centre de recherche Paul-Pascal–CNRS, 115 avenue du Docteur-Schweitzer, F-33600 Pessac, France

² Universidade de São Paulo, Instituto de Física-GFCx, P.O.B. 66318, São Paulo, SP 05314-970, Brazil

Received 20 May 2011

Published online: 29 August 2011 – © EDP Sciences / Società Italiana di Fisica / Springer-Verlag 2011

Abstract. The structure of a complex between hydrated DNA and a non-cationic lipid is studied, including its phase diagram. The complex is spontaneously formed by adding DNA fragments (ca. 150 base pairs in length) to non-cationic lipids and water. The self-assembly process often leads to highly ordered structures. The structures were studied by combining X-ray scattering, fluorescence and polarized microscopy, as well as freeze-fracture experiments with transmission electron microscopy. We observe a significant increase of the smectic order as DNA is incorporated into the water layers of the lamellar host phase, and stabilization of single phase domains for large amounts of DNA. The effect of confinement on DNA ordering is investigated by varying the water content, following three dilution lines. A rich polymorphism is found, ranging from weakly correlated DNA-DNA in-plane organizations to highly ordered structures, where transmembrane correlations lead to the formation of columnar rectangular and columnar hexagonal superlattices of nucleotides embedded between lipid lamellae. From these observations, we suggest that addition of DNA to the lamellar phase significantly restricts membrane fluctuations above a certain concentration and helps the formation of the lipoplex. The alteration of membrane steric interactions, together with the appearance of interfacial interactions between membranes and DNA molecules may be a relevant mechanism for the emergence of highly ordered structures in the concentrated regime.

1 Introduction

Under proper conditions, surfactants can be used for preparing nanostructured materials thanks to their ability to self-assemble into a variety of liquid crystalline phases. Lamellar phases are particularly attractive for preparing layered composite structures because colloidal particles can be intercalated within or between surfactant bilayers. The final properties of the composite can be controlled by varying the bending rigidity of bilayers or their separation. The design and preparation of a variety of new composite materials open a broad horizon for several technological applications, covering fields from materials science to biomedicine [1] and offer new challenges in understanding self-assembly in soft-confined geometries [2,3]. In this context, synthetic vectors for gene therapy based on “lipoplexes”, *i.e.* complexes prepared with (cationic) lipids and DNA have been proposed as an alternative to viral vectors [4–6].

The transfection efficiency of a cationic lipoplex depends on several parameters involved in preparation protocols such as quantity of DNA and cationic lipids—usu-

ally at charge ratio 1:1—, incubation time and mixing conditions [7]. Therefore, the feasibility of these carriers depends on understanding the mechanism responsible for the formation of the complex and their physical properties, either to optimize the quantity of material to be encapsulated or to provide release into the targeted cells [8].

Structural properties of lipid-DNA complexes have been investigated by X-ray diffraction and electron microscopy techniques [9,10]. One of the most commonly found structures is the one in which DNA molecules are intercalated in the water gaps of multilamellar stacks of lipid bilayers. Such symmetry was first observed by Rädler *et al.* using cationic lipids (CLs) complexed with linear DNA [11]. In this pioneer work, it was proposed that the hosted (rod-like) particles form locally ordered structures with an interaxial spacing depending on a delicate interplay between the charges of the anionic polyelectrolyte and the positive membrane. Since then, numerous studies have been conducted and other superstructures have been evidenced over the last years. For example, the formation of columnar centered-rectangular DNA lattices embedded in L_β^c phases of CLs was found to be related to the thermotropic behavior of the DMPC/DMTAP lipid mixture [12,13]. A similar structure was also observed in non-cationic (zwitterionic) complexes after long-term incubation and in the presence of divalent counterions [14,15].

^a Present address: Universidade de São Paulo, Instituto de Física-GFCx, São Paulo, Brazil.

^b e-mail: navailles@crpp-bordeaux.cnrs.fr

Although more frequent, lamellar structures of lipids hosting DNA strands are not the unique conformation found in lipoplexes. Inverted hexagonal phases of lipids containing DNA rods inserted in cylinders of water (H_{II}^c) [16,17] and micellar honeycomb structures of lipids hosting nucleotides in the interstices of the phase have also been reported [18,19]. In this last case, nucleic acids form a hexagonal supramolecular arrangement (H_I^c).

At theoretical level, several models, most of them based on electrostatic interactions, have been proposed in order to address the above-described self-assembly [20, 21]. Computer simulations, either at atomistic scale or based on effective potentials, have also been used in attempts to bring insights into these systems [22–24]. A variety of equilibrium mesophases, some of which not yet experimentally found, has been predicted and some light on the fundamental mechanisms involved in complexation has emerged from these approaches [25,26]. However, in the case of entirely non-cationic lipids such as studied here, it is very rare to find works addressing the question from a theoretical point of view. This lack may be due to long-term belief that DNA complexation was possible only with positively charged lipids, or with the help of multivalent (small) cations for mediating lipid-DNA association [14,27], though (small) ions and, in particular, anions have been reported to interact with zwitterionic membranes [28,29]. In fact, the formation of DNA–neutral-lipid complexes was experimentally demonstrated [30,31]. A Flory model has also been proposed in order to explain the phase behavior in such systems [32].

In a previous work [33], we demonstrated experimentally the existence of a hexagonal superlattice in a hydrated-DNA–non-cationic-lipid complex prepared without counterion mediation. The identification of such structure was enabled by X-ray diffraction in grazing-incidence geometry on oriented supported films. The evolution of supramolecular structure was followed *in situ* as the sample was dehydrated in a controlled humidity chamber. A major drawback of this approach is the lack of knowledge about the exact water amount in the system and the fact that the film, initially very hydrated, is to be progressively dehydrated ideally in thermodynamic equilibrium with a reservoir, a condition whose implementation can be questioned in the case of bulk samples.

The design of lipoplexes requires the establishment of phase diagrams, including the identification of the different structures with their respective domains and the description of phase separations. This experimental approach, ideally combined with theoretical studies, may yield more detailed description of intermolecular interactions. In the current work we explore the phase diagram of a non-cationic-lipid–DNA complex, along three dilution lines, by preparing samples separately with distinct amounts of water. The precise control of water content in each sample allows us to follow the evolution of supramolecular structure as a function of hydration.

We observed the formation of 2D hexagonal lattices of DNA for very dehydrated samples, in bulk, similarly to what was observed in thin films, in addition to other structures, like a columnar rectangular lattice of DNA

rods embedded in lamellar phases of lipids, in strongly dehydrated domains. We noted also the presence of DNA–DNA in-plane correlations, characterized as a nematic-like organization of nucleotides between lamellae, for more hydrated samples. The formation of single-phase domains was found to be closely related to the presence of *large* quantities of DNA in the system, suggesting the relevance of packing constraints and short-range repulsive forces to the formation of the complex.

2 Materials and methods

2.1 Sample preparation

Calf thymus DNA was purchased from Sigma-Aldrich and desalted with a buffer solution (sodium acetate 3 M, pH adjusted to 5.2, also from Sigma-Aldrich) mixed to pure ethanol, following the standard precipitation procedures: After freezing overnight at -20°C , the mixture was centrifuged and the supernatant removed. The pellet was then washed three times with a 70% ethanol solution and centrifuged. The precipitate was finally subjected to lyophilization, yielding salt-free nucleotides (apart from sodium counterions neutralizing the DNA phosphate groups) for sonication. The ultrasound treatment (followed by the intercalation of YOYO fluorescent dye) led to pieces with ca. 150 bp and contour length of ca. 50 nm. This size roughly corresponds to the persistence length of the biopolymer and allows describing the fragments as rigid rods. If hydration shells are not taken into account, the rod diameter is 2 nm. The lipid part was composed by soya lecithin-phosphatidylcholine (PC) and Simulsol, a non-ionic co-surfactant of pharmaceutical grade that is a mixture of ethoxylated fatty acids derived from oleic acid (71%) and palmitic acid (11%) as main components. The products were purchased from Sigma and Seppic, respectively, and used without further purification. They were cosolubilized in cyclohexane at PC-to-Simulsol mass ratio of 7:3 and desiccated under lyophilization overnight in order to evaporate the solvent. The role of the helper surfactant was to increase the flexibility of the formed lamellae, enlarging the dilution domain of the host phase. Due to the zwitterionic character of lecithin headgroups, and non-ionic nature of Simulsol, the overall charge of the resulting membrane, though locally bearing electric dipoles, was neutral. Henceforth, the preparation PC+Simulsol will be referred to just as *lipids*. Samples were prepared by mixing DNA fragments, lipids and water into clean Eppendorf tubes. We have chosen three lipids-to-DNA volume ratios ($\rho = \phi_{ip}/\phi_{DNA}$), namely 3.1, 5.1 and 8.1. The amount of water (ϕ_w) was varied while ρ was kept constant in such a way that dilution lines were followed on the phase diagram. After the preparation of the tubes, they were stored under refrigeration at 4°C . In order to ensure homogenization and to reach thermodynamic equilibrium, samples were submitted to daily centrifugation with alternating upside down cycles. This treatment was carried out for at least 4 weeks before any further analysis.

2.2 X-rays experiments

Once having reached equilibrium, samples were carefully transferred at room temperature into sealed glass capillaries, which usually yields randomly oriented domains. High-flux and high-resolution X-ray experiments were carried out on the SWING beamline at the synchrotron facility SOLEIL near Paris, France. With a sample-to-detector distance equal to 1575.6 mm and radiation wavelength $\lambda = 0.103$ nm, the scattering wave vectors in reciprocal space ranged from $q = 0.6$ nm⁻¹ to $q = 6.0$ nm⁻¹. The total resolution of detection was estimated by fitting Lorentzian functions to peaks from silver behenate diffractograms. The value of $\Delta q/q$ was found to be ca. 1.7×10^{-2} at 2 nm⁻¹. The beam size at the sample position was 0.4×0.1 mm ($H \times V$). Images were captured by the Avix170170 CCD detector. Data were radially averaged and background intensities were subtracted. Reduction was performed by using the software *Foxtrot*, an application developed by the SWING beamline staff.

Complementary X-ray data were collected employing conventional sources installed at the Centre de recherche Paul-Pascal. A Bruker Nanostar machine was used to obtain scattering profiles in q range between 0.4 nm⁻¹ and 8.0 nm⁻¹. The sample-to-detector distance was 250 mm and the radiation wavelength was $\lambda = 0.154$ nm. Spectra were registered on the Bruker gas-based detector HiStar, providing a uniform and low background noise, which was subtracted during data treatment with *Fit 2D* software. The total resolution, at 2 nm⁻¹, was $\Delta q/q \approx 6.3 \times 10^{-2}$.

A home-made, rotating-anode-based setup was used to evaluate the scattering profile in the wide angle region. The goal of such experiments was to probe the fluidity of aliphatic chains within the lipid bilayers. The sample-to-detector distance was 133 mm and, with radiation wavelength $\lambda = 0.154$ nm, q ranged from 2.0 nm⁻¹ to 22.0 nm⁻¹. The detection system is a Marresearch image plate coupled to an on-line scanner, leading to total resolution $\Delta q/q \approx 8.1 \times 10^{-2}$ at 2 nm⁻¹.

All above-described experiments were carried out on thermally equilibrated samples at 25 °C, which was obtained by keeping the sample holders under water circulation at controlled temperature.

2.3 Optical observations

Optical microscopy was performed with a Leica DM IRE2 inverted epifluorescence microscope. Samples were sandwiched between microscopy slides and coverglasses, submitted to gentle manual shearing in order to obtain thin samples and then sealed with a UV-curing glue. Birefringent textures were inspected by illuminating with polarized light and observing through a crossed analyzer. Fluorescence observations were carried out by using a blue/green filter cube, suitable for the 491 nm/509 nm YOYO dye used for the labeling of DNA rods. Magnifications were chosen to be 10× or 40× allowing visualization of large domains within an area of a few mm². Images were captured with a CooledSNAP HQ CCD camera controlled by *MetaMorph* software (Molecular devices, version 7.5).

2.4 Freeze-fracture and electron microscopy

Replicas for transmission electron microscopy were prepared according to standard freeze-fracturing protocols [34]. Small quantities from preparations were deposited in gold stubs and plunged into liquid-nitrogen bench dewars containing liquid propane cooled to -190 °C. Thereupon, samples were introduced in a BALTEC machine BAF060 under an atmosphere of 10⁻⁹ bar at temperature of -150 °C. Fracturing was accomplished by passage of cold microtome knife through the frozen specimen, preserving internal structures. The system was replicated by shadowing a 4 nm Pt-C film sputtered at an angle of 45°. A second carbon layer, with a thickness of 30 nm, was finally deposited normal to the surface. The replicas were mounted on cooper grids after being removed from the gold holders by successive baths in ethanol/water and chloroform/ethanol mixtures. Observations were carried out with a Hitachi H600 transmission electron microscope.

3 Results and discussions

3.1 Lipid-water system: host phase

In a first stage, we characterized the host phase (lipid/water system). The main goals were to evaluate the dilution domain and to determine the hydration limit as well as the thickness of the bilayers and their fluidity. Using both SAXS and WAXS, we obtained diffractograms for water volume fractions situated between $\phi_w \approx 0.30$ and $\phi_w \approx 0.75$. Multilamellar stacks of regularly spaced bilayers were found throughout the studied domain. Figure 1A, shows two selected $I(q)$ vs. q plots from the binary system for lipid volume fractions equal to 0.70 and 0.45. As the water amount increases, the Bragg peaks shift towards small angles, indicating the swelling of the lamellar phase. For concentrated samples, *e.g.* $\phi_{lip} = 0.70$, up to four narrow Bragg reflections are observed, attesting strong ordering and a large number of correlated bilayers in single domains. For diluted samples, the number of visible Bragg peaks decreases while peaks broaden, indicating a lesser strength of the smectic ordering (softer elastic properties and decrease in number of correlated bilayers) as the system approaches full hydration. The systematic presence of a broad peak around $q = 14$ nm⁻¹ (inset in fig. 1A) evidences the fluid state of the lipid bilayers (*i.e.* the L_α phase) throughout the whole dilution domain.

Parallel to X-ray analysis, we carried out observations with a polarizing microscope. Homogeneous lamellar textures were found with most samples (fig. 1B). Exceptions were observed in very hydrated preparations ($\phi_w > 0.60$), with occurrence of droplets due to the water in excess. In order to complement structural data, we also performed freeze-fracture replicas and transmission electron microscopy (TEM) imaging. Large defect-free smectic domains (fig. 1C) were found and Fourier image analysis revealed a strong one-dimensional anisotropy with lamellar periodicities in excellent agreement with X-ray measurements.

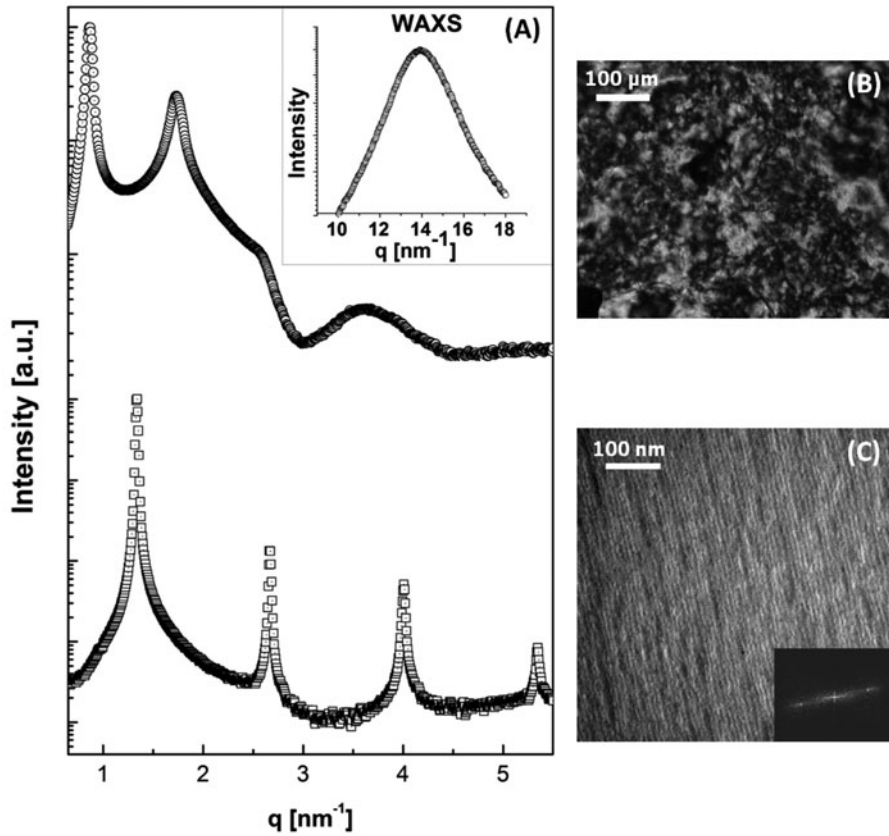


Fig. 1. (A) Selected diffractograms from the binary system, with $\phi_{lip} = 0.45$ (\circ) and 0.70 (\square). Inset: broad peak around $q = 14 \text{ nm}^{-1}$, characteristic of the fluid state of aliphatic chains in the lipid membranes. (B) Typical lamellar texture under light-polarized microscopy. (C) Freeze-fractured replica showing a plane nearly perpendicular to lamellae. Fourier analysis (inset) shows a strong one-dimensional anisotropy, with repetition distance $D = 5 \text{ nm}$ in excellent agreement with 4.9 nm from X-ray data (not shown) for $\phi_{lip} = 0.75$.

The study of the behavior of lamellar periodicity as a function of the amount of water allowed us to identify two distinct regimes. The first one was found to be consistent with the usual one-dimensional swelling law, until a water volume fraction $\phi_w \approx 0.60$ is reached. In this interval, lamellar periodicities range from 5 nm to 9.2 nm . The usual relationship between the smectic spacing and hydration in the form $D = \delta_m / (1 - \phi_w)$, with δ_m corresponding to the bilayer thickness, was found. Performing a least-square fit over data from this domain, we determined the bilayer thickness to be $\delta_m = 3.7(1) \text{ nm}$. In the second domain, for $\phi_w \geq 0.60$, the system phase-separated with water in excess and a plateau value around $9.2(5) \text{ nm}$ was found for D . The information about the membrane thickness enables us to obtain the height of the aqueous layers ($d_w = D - \delta_m$), *i.e.* the available space for hydrophilic nucleotides. Figure 2 shows the behavior of the intermembrane spacing d_w as a function of the lipid volume fraction. Horizontal dotted lines indicate the dilution limit and the DNA diameter, a geometrical limit below which the thickness of aqueous layers is not large enough to accommodate DNA molecules viewed as cylindrical objects. The region between the lines corresponds to the range where a (homogeneous) host phase is able to incorporate DNA rods.

3.2 Lipid-DNA-water system: structural polymorphism

In a second stage, we prepared DNA-containing samples following the procedure described in the materials and methods sect. 2.1. Unlike most studies reported in the literature, where the complexes are prepared in excess of water, here we used the swelling properties of the host lamellar phase in order to control the soft confinement and to drive the nucleotide organization in the complexes. Hydration was varied in such a way that the water layers had thicknesses ranging between the DNA diameter and the dilution limit. The structure of the complex at mesoscopic and molecular scales was followed by SAXS and WAXS. Addition of DNA did not change the fluid (L_α) state of the membranes. The diffuse peak at $q \approx 14 \text{ nm}^{-1}$ was observed for all samples. In fig. 3, we show selected diffractograms from two single-phase domains found along the dilution line $\rho = 3.1$, for lipid volume fractions equal to 0.48 and 0.63 , respectively.

In the more hydrated domain (fig. 3, top), the scattered intensity as a function of the wave vector modulus q exhibits 4 Bragg reflections at positions $q_n = 2\pi(n+1)/D$ arising from a lamellar stack with the repeat distance D equal to 7.1 nm in this example. Under polarized light, the typical birefringent texture for lamellar phases is observed.

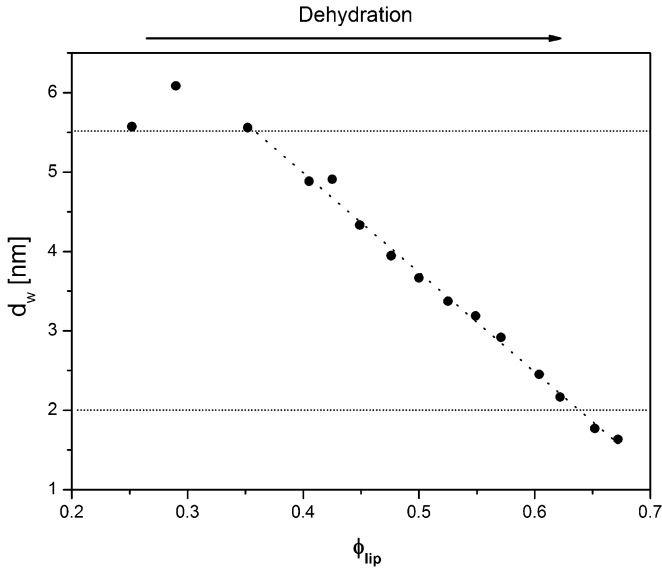


Fig. 2. Behavior of the intermembrane spacing d_w as a function of lipid volume fraction ϕ_{lip} . The range of available distances for incorporation of nucleotides is indicated by the two horizontal dotted lines corresponding to the dilution limit and DNA diameter, respectively.

In addition, fluorescence microscopy reveals homogeneity of the fluorescence intensity on the images, which points to a homogeneous distribution of the DNA molecules incorporated inside the lamellar phase (data not shown). Apart from the 4 regularly spaced Bragg reflections, samples with lipid volume fractions ranging between 0.44 and 0.53 also show a broad peak between the second and the third lamellar orders. This peak is associated with DNA-DNA correlations and, in the example of fig. 3, the average distance between nucleotides is found to be ca. 2.9 nm.

A possible organization to explain the observed data is an orientational ordering of the DNA in the plane of membranes (L_α^N). In this case, owing to in-plane rod-rod and out-of-plane rod-membrane excluded-volume interactions the rods form a nematic bidimensional mesophase, without positional ordering or transmembrane correlations. Another satisfactory hypothesis, however, places DNA molecules into regular galleries forming a 2D smectic structure in the plane of bilayers without transmembrane correlations [35]. A third possible interpretation is to consider, besides in-plane correlations, some degree of layer-to-layer orientational ordering. This last case could imply the presence of the so-called “sliding phase”, theoretically predicted but not experimentally found yet (L_α^S) [25,26]. Unfortunately, none of these different models can be excluded from an analysis of SAXS spectra obtained with *powder* samples (the case of the present study). In order to overcome this drawback, an alternative insight could be a modeling of the scattering curves taking into account variations of electron density profiles for distinct types of orientational and positional ordering of the DNA molecules inside the host lamellar phase. Such models would allow the deconvolution of the form factors for different orga-

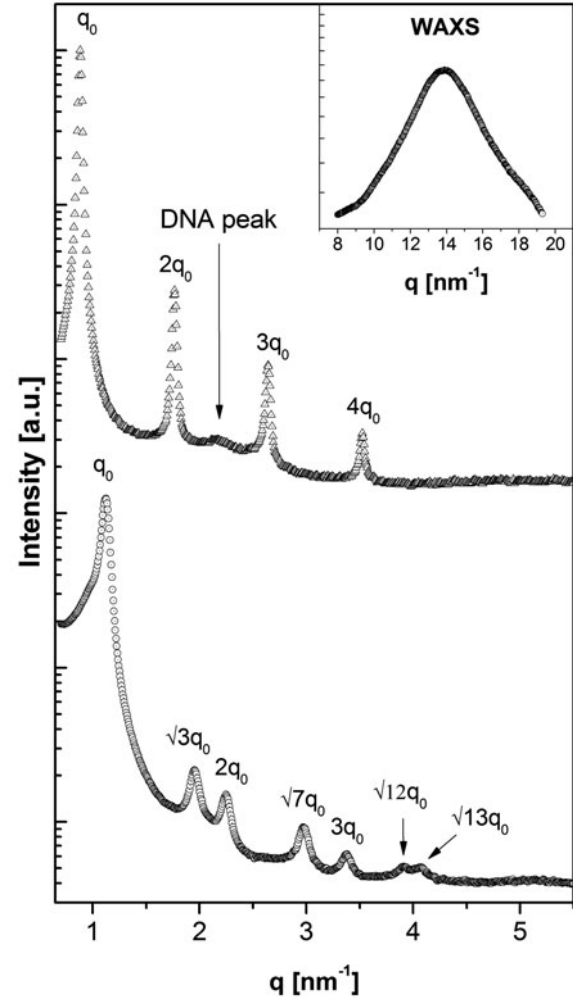


Fig. 3. Selected scattering data for homogeneous DNA-containing samples with nematic (Δ , top, $\phi_{lip} = 0.48$) and hexagonal (\circ , bottom, $\phi_{lip} = 0.63$) organization of DNA inside lamellar host phases. The broad peaks systematically found at $q \approx 14 \text{ nm}^{-1}$ (inset) indicate a fluid state for the aliphatic chains in the lipid bilayers.

nizations, making it possible to distinguish the different structures. However, as far as we know, such studies have not been successfully realized to date.

Measuring the half-width at half maximum ($\Delta q/2$) of diffuse peaks fitted with Lorentzians functions (data not shown), we estimated typical correlation lengths ranging from 6 to 15 aligned DNA molecules. This yields weak correlations between particles, reinforcing the hypothesis of a nematic arrangement for nucleotides [36]. We were able to develop a simple geometric model in order to better ascertain the validity of this hypothesis. In fig. 4, we present a schematic drawing of the proposed 2D unit cell for the DNA organization in hydrated, single-phase domains. The model is constructed taking into account the structural parameters from X-ray data (lamellar periodicity and average distance between rods) and the previously known membrane thickness and DNA diameter. From simple geometric considerations (assuming flat bilayers, *i.e.*

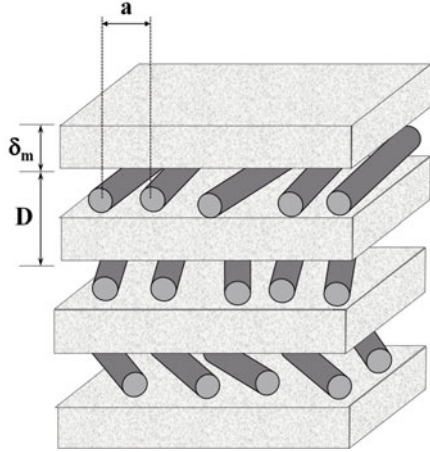


Fig. 4. Schematic representation of a nematic organization of DNA rods between lipid bilayers (L_α^N). D represents the lamellar periodicity of the host phase and a is the average distance between DNA molecules, both obtained from X-ray data.

neglecting undulation fluctuations or the presence of defects), we derive eqs. (1)–(3) which allow us to predict the relevant volume fractions describing the composition of the system:

$$\phi_{DNA} = \frac{\pi\Phi_{DNA}^2}{4Da}, \quad (1)$$

$$\phi_{lip} = \frac{\delta_m}{D}, \quad (2)$$

$$\phi_w = 1 - \phi_{DNA} - \phi_{lip}, \quad (3)$$

where ϕ_{DNA} , ϕ_{lip} and ϕ_w are the volume fractions for DNA, lipids and water, respectively. Φ_{DNA} is the diameter of rods and δ_m , the thickness of the membranes. D and a are the lamellar periodicity and the average distance between cylinders.

As the experimentally formulated volume fractions are *a priori* known for water, lipids and DNA, it is possible to compare the geometrical predictions with formulated quantities. In fig. 5, we present a comparison between the experimental and predicted volume fractions for all the samples exhibiting the (nematic) DNA peak. Lines represent theoretical predictions from expressions (1)–(3), while symbols indicate the experimentally formulated volume fractions for lipids, water and DNA. As is clear from the graph, there is a very good match between experimental data and theoretical predictions, underlining the reliability of the model.

In the second single-phase domain along the dilution line with $\rho = 3.1$, we observe Bragg peaks corresponding to a 2D hexagonal symmetry (fig. 3, bottom). The system is highly organized such that reflections at positions $q = \sqrt{12}q_0$ and $q = \sqrt{13}q_0$ can easily be identified. Inspection under polarizing microscopy showed only the presence of *lamellar* textures, while fluorescence microscopy revealed a homogeneous distribution of the DNA within the lipid phase. The Bragg peak component of

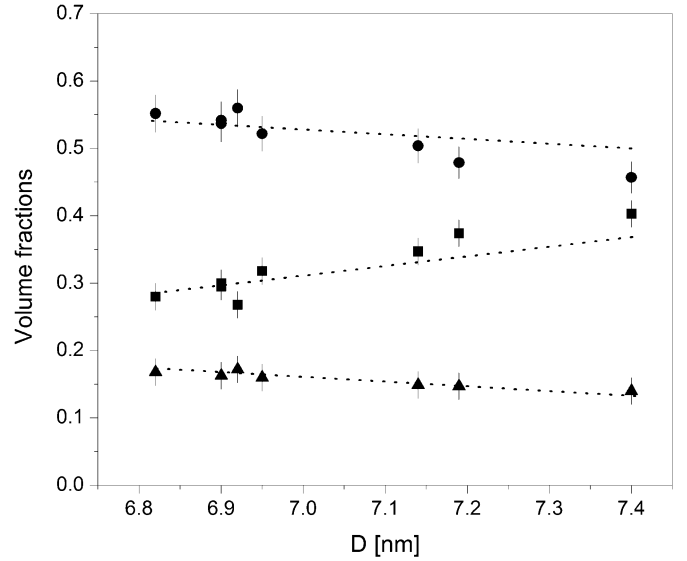


Fig. 5. Experimental and predicted volume fractions for all the samples exhibiting the (nematic) DNA peak. Lines represent theoretical predictions from expressions (1)–(3) and filled symbols (circles for lipids, squares for water, triangles for DNA) indicate the experimentally formulated volume fractions.

the X-ray spectra again allows multiple interpretations. In fig. 6, we present two candidate structures which adequately describe the 2D hexagonal symmetry of the observed diffraction pattern. In the first one (fig. 6A), DNA rods form a hexagonal lattice inserted inside the water layers of a (direct) lamellar phase of lipid membranes (L_α^H). In the second sketch (fig. 6B), the lipid component forms an inverted hexagonal structure, where DNA fragments are inserted into cylinders of water (H_{II}^c phase). The expressions deduced in eqs. (1)–(3) are general for platelet structures hosting cylinders and are valid to describe the scheme drawn in fig. 6A. For the H_{II}^c symmetry, the prediction for ϕ_{DNA} also remains the same. The expressions for ϕ_w and ϕ_{lip} are quite different, however, and now read

$$\phi_w = \frac{\pi(a - \delta_m)^2}{4aD} - \phi_{DNA}, \quad (4)$$

$$\phi_{lip} = 1 - \phi_w - \phi_{DNA}. \quad (5)$$

Note that, in writing eq. (4), we add a (presumably non-restrictive) hypothesis, namely that the membrane thickness δ_m is identical to the size of the lipid domains along the natural hexagonal directions.

In fig. 7 we plot the geometrical predictions derived from eqs. (2)–(5) and compare them with the experimental lipid and water volume fractions. In spite of some deviations in both cases, we observe a better agreement between experimental data and theoretical predictions for the L_α^H hypothesis. This result is in good agreement with those published previously on oriented supported films [33]. The obtained lattice parameters a are around 6.5 nm which corresponds to lamellar periodicities of $D = \sqrt{3}a/2 \approx 5.6$ nm. Subtracting the geometrical thickness of the bilayers, the available space for DNA is ca. 1.9(1) nm, slightly

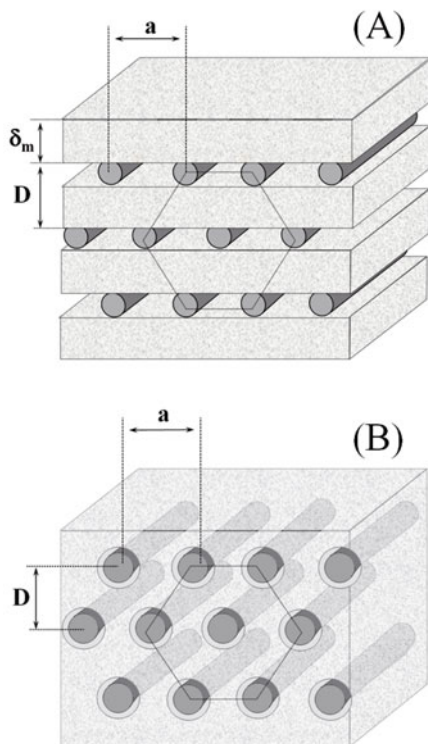


Fig. 6. Schematic representations corresponding to (A) L_α^H and (B) H_{II}^c hypotheses, both compatible with the sets of Bragg peaks observed in the dehydrated region of the phase diagram.

below the geometrical limit and thus requiring (small) deformations of the membranes. It should be noted again that bilayers were considered here to be completely flat: Static deformations could explain the deviations from the model.

In order to obtain direct observation of this lamellar phase with hexagonal organization of the DNA molecules, we performed freeze fracture experiments and transmission electron microscopy. Far from the concentrated domain (L_α^H phase), the picture is typical of a regular smectic (data not shown). We observe, as for the host phase without DNA, flat layers separated by abrupt steps which are fractured along the stacking axis—see fig. 1C for an example. Closer to the L_α^H phase, the fracture occurs more frequently in the plane of the layers, but no special feature is observed. In fig. 8A, we present an overview image showing an area of ca. $1 \mu\text{m}^2$ for a sample in the L_α^H domain, with $\phi_{lip} = 0.63$ and $\rho = 3.1$. Numerous anisotropic patterns are visible in the layer plane (fig. 8B). These rod-like structures are typically $53 \text{ nm} \times 3 \text{ nm}$ in size, in rather good agreement with the expected size for 150 bp DNA molecules taking into account the shadowing layer. The resolution limit of freeze-fracture technique, which is estimated to be ca. 2 nm for *periodical structures* [10], does not allow accurate measurements of the DNA diameter. However, the shape of the molecules can be outlined as observed before in similar contexts [37–39]. At a larger scale (fig. 8A), coexisting domains of rod-like structures and layer jumps (white arrows) can be observed, thus confirm-

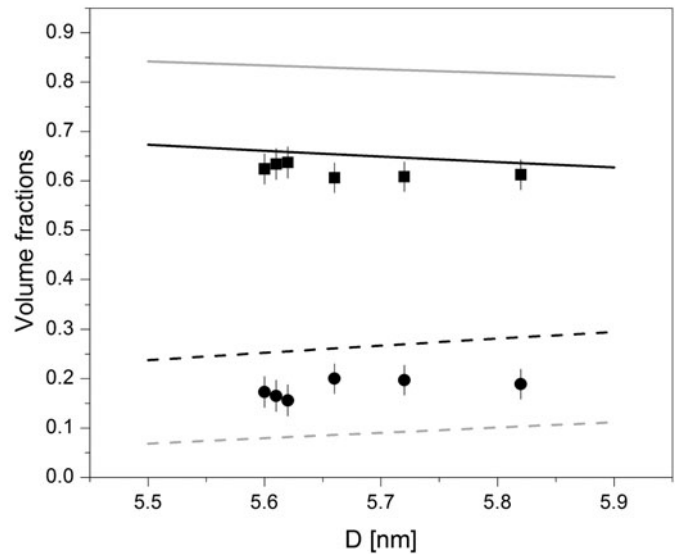


Fig. 7. Comparison of ϕ_{lip} (filled circles: experimental values) and ϕ_w (filled squares) for the 2D hexagonal structures sketched in fig. 6. Solid lines indicate predictions for lipid volume fractions, and dashed lines for water volume fractions. L_α^H predictions are represented in black, whereas H_{II}^c are showed in gray.

ing the presence of a lamellar layering. Moreover, separations between rod-like structures are found to be 6.1 nm, in good agreement again with a DNA-DNA separation equal to 6.5 nm obtained from X-rays. Image analysis, performed by Fourier transforms (fig. 8C), suggests the conservation of layer-to-layer orientation, in accordance with the expected behavior for a L_α^H structure.

In fig. 9 we show the behavior of structural parameters, as a function of the lipid volume fraction along the whole dilution line with $\rho = 3.1$. The lamellar repeat distance is represented by squares, whereas circles are associated to the distance between DNA rods. The approximate boundaries between different domains are indicated by vertical dashed lines. In the more hydrated domain (ϕ_{lip} less than ca. 0.53), the periodicity of the host phase present a quasi-linear dependence on hydration, quite similar to the behavior observed for the DNA-free system. It is possible to identify lamellar spacings between 6.8 nm and 7.2 nm, leading to aqueous layers between 3.1 nm and 3.5 nm. This space is sufficiently large to accommodate one layer of DNA rods, without need for deforming the lipid bilayers. In turn, the interaxial spacing between DNA molecules, obtained from the position of the diffuse peak between the second and third lamellar orders, is found to decrease slightly with the confinement imposed by the host phase until it reaches a minimum value around 2.6 nm. Such a value, somewhat larger than the DNA diameter, appears to be large enough to accommodate a few hydration shells around the DNA rods.

In the highly ordered domain (ϕ_{lip} larger than ca. 0.60), both lamellar periodicity and DNA-DNA distances became nearly constant, around $D = 5.6 \text{ nm}$ and $a = 6.5 \text{ nm}$, respectively. These values seem to be characteristic of the more compact structure allowed in the system.

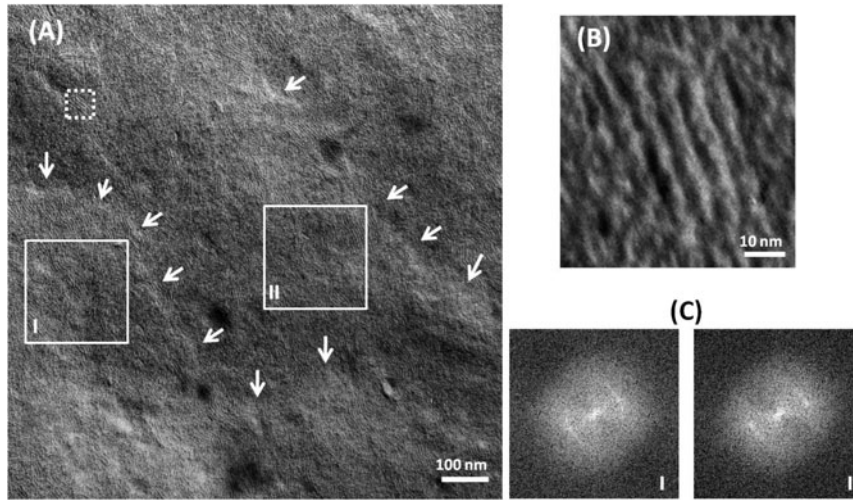


Fig. 8. Electron microscopy images over freeze-fractured replica from L_{α}^H phase. (A) White arrows point at smectic steps delimiting planes along which DNA rods appear to be highly oriented. (B) Detail from dashed square in panel (A), showing rod-like structures with dimensions (length and separation) in close agreement with those expected for DNA. (C) Fourier transforms over solid squares indicated in panel (A), revealing coherence of layer-to-layer orientation, as predicted for L_{α}^H phases.

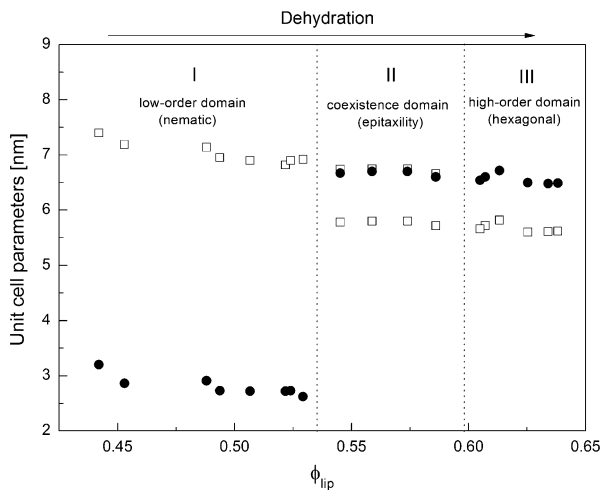


Fig. 9. Behavior of the structural parameters as a function of the lipid volume fraction. Squares represent the smectic spacing of the lipid host phase, circles the separation between DNA rods. Dotted lines: guide for the eyes representing the approximate location of the boundaries between domains.

Deformations of the membranes are also consistent with FFTEM observations presented in fig. 8. It is interesting to note that the distance between DNA molecules is significantly *larger* than the one observed in the dilute regime (L_{α}^N), and also in the hexagonal phase of the DNA-water binary system studied by Livolant and co-workers [40]. These observations suggest the existence of repulsive interactions between DNA molecules when the layer-to-layer orientational correlations appear in the L_{α}^H phase. These findings point to strong excluded-volume interactions between DNA and membranes, as will be discussed below.

Between the two above-described single-phase domains, a coexistence region is found. In fig. 10 we present a selected spectrum for a sample in this region of the phase

diagram, with volume fractions $\phi_{lip} = 0.59$, $\phi_{DNA} = 0.19$ and $\phi_w = 0.22$. The observed Bragg peaks are easily indexed as corresponding to two distinct phases, one associated to the previously mentioned 2D hexagonal symmetry, in coexistence with a second lamellar phase where rods are found to exhibit a nematic-like organization, as pointed out by the typical diffuse peak between the second and third lamellar orders. Light-polarized microscopy reveals only the existence of lamellar textures. Under fluorescence (showed in the inset of fig. 10), the system appears to be inhomogeneous, varying fluorescence intensities indicating regions with rather different DNA concentrations, but confirming the presence of DNA in the two coexisting phases. A remarkable property for samples within the two-phase domain is the approximate identity between the lattice parameter a associated to the hexagonal symmetry with the periodicity of the coexisting lamellar phase. This epitaxy remains unexplained.

3.3 Other dilution lines

Two other dilution lines ($\rho = 5.1$ and $\rho = 8.1$) were also scanned in the same manner. In general, a rich polymorphism was found, with low order at high hydration and the emergence of highly organized domains at lower water content. For these ρ values, it was not possible to observe single-phase domains, except for two formulations along the line $\rho = 5.1$ ($\phi_{lip} = 0.53$ and $\phi_{lip} = 0.37$) which were found to be L_{α}^N phases. The phase boundary may be close to the nominal composition corresponding to the sample with $\phi_{lip} = 0.53$ at $\rho = 5.1$, and smaller steps in ρ should be investigated in order to clarify this apparent “re-entrant” behavior. The remaining structures were systematically found in coexistence. Polarization microscopy showed lamellar textures in all the investigated hydration

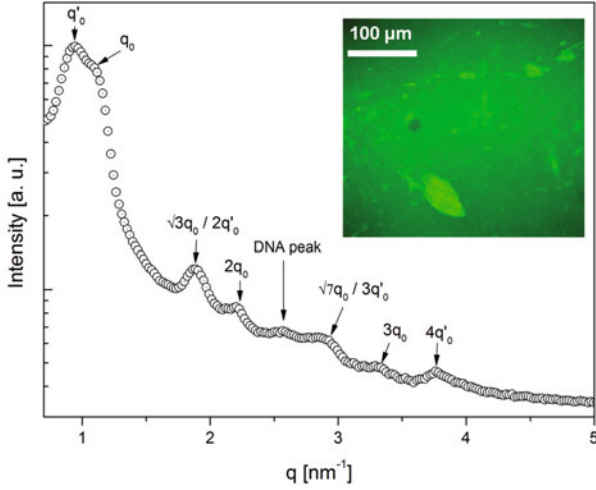


Fig. 10. Selected diffractogram from the coexistence region for a sample with overall composition $\phi_{lip} = 0.59$ and $\rho = 3.1$. A 2D hexagonal symmetry is found with a lattice parameter a epitaxially matched with the periodicity of the lamellar phase in coexistence, also containing weakly ordered DNA rods. Inset: Fluorescence images (color on-line) showing domains with distinct nucleotide concentrations.

range, pointing to the persistence of a smectic-like assembly for the lipid phases. In fluorescence microscopy, it was possible to identify either a coexistence between DNA-containing and DNA-free lamellar phases, or the simultaneous presence of nucleotides in both lamellar phases. Apart from nematic and hexagonal organizations found before, these dilution lines also revealed in the dehydrated range families of Bragg peaks that could be indexed according to $q_{hk} = 2\pi[(h/a)^2 + (k/b)^2]^{1/2}$, and presumably corresponding to columnar simple rectangular lattices of DNA. In fig. 11, we display the complete experimental phase diagram, as studied here, wherein the formation of single-phase domains is observed for DNA-rich domains only.

The question of why the DNA is incorporated completely only for *large* amounts of nucleotides is an interesting one because, in contrast with cationic lipid systems, here electrostatics is not an obvious candidate to drive complexation. The globally neutral charge of lecithin headgroups as well as the neutrality of the helper surfactant requires more subtle mechanisms, possibly including ion-dipole interactions [28,29], to explain the formation of the complex. The question was theoretically addressed partially before, in terms of a Flory approach (*i.e.* enthalpic penalty) to deal with (entropic) anisotropic excluded-volume effects: The authors of ref. [32] managed to develop a theoretical phase diagram which is in reasonable agreement with our experiments. Unfortunately, the model does not include a description of the *dry* region where highly ordered superlattices are found. This difficulty in dealing with dehydrated domains is partially due to the restriction of undulations in strongly confined geometries, as well as to strong, short-range interactions other than steric repulsion becoming increasingly rele-

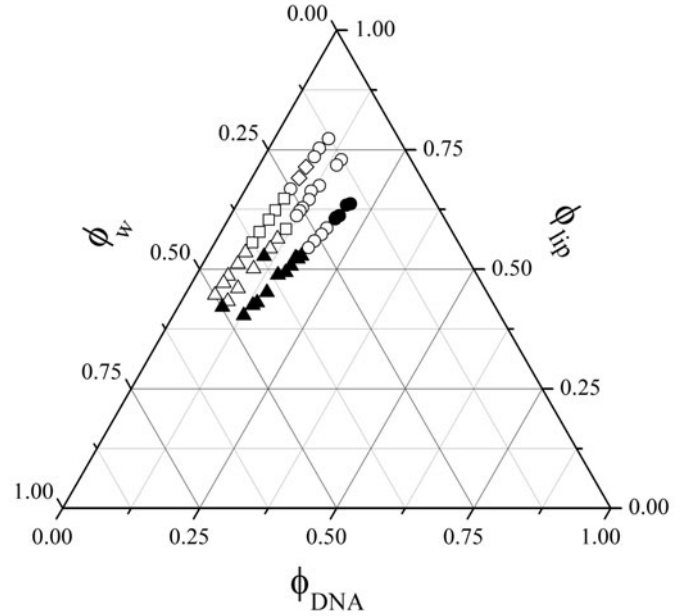


Fig. 11. Complete phase diagram resulting from the present work. Monophasic domains were systematically observed along the line $\rho = 3.1$ only, in qualitative agreement with the theoretical predictions from ref. [32]. Solid symbols indicate single-phase points: $\blacktriangle = L_\alpha^N$, $\bullet = L_\alpha^H$. Open markers represent phase coexistence: $\triangle = L_\alpha^N + L_\alpha^N$ or $L_\alpha^N + L_\alpha$, $\circ = L_\alpha^H + L_\alpha^N$ or $L_\alpha^H + L_\alpha$, $\diamond = L_\alpha^H + L_\alpha^R$, $\square = L_\alpha^N + L_\alpha^H$ or $L_\alpha + L_\alpha^H$.

vant. For strongly confined complexes, the thickness of the aqueous layers is very close indeed to the diameter of DNA rods. This proximity increases steric and other short-range interactions between bilayers and nucleotides, as well as between nucleotides themselves, in such a way that a model consistently describing the system must compulsorily take into account their interplay, which is at present beyond the available Flory approach.

3.4 Effects of DNA on the smectic ordering of the lipid phase

Besides the formation of polymorphic superlattices embedded between bilayers, we observed that the introduction of DNA has dramatic effects on the ordering of the lipid phase. In fig. 12, we present a comparison between two spectra from samples with and without nucleotides but with approximately the same lamellar periodicity. One can note that, in spite of the latter similarity, the DNA-containing phase is significantly more ordered than the host phase without DNA. This increase in smectic ordering is clearly evidenced by the appearance of the third and fourth lamellar orders, together with a narrowing of the Bragg peaks. Diffuse scattering is remarkably distinct, too. While in the binary system there is a form factor broad maximum around $q \approx 3.7 \text{ nm}^{-1}$, in the ternary complex this region is quite distinct, with a very strong reflection

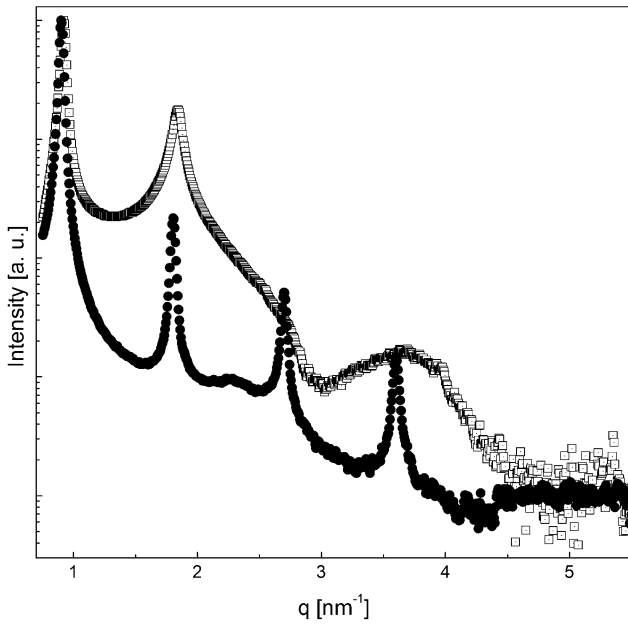


Fig. 12. Comparison between spectra from samples with and without DNA. Filled circles represent the DNA-containing system while open squares correspond to a DNA-free system with an equivalent lamellar periodicity ($D \approx 6.8$ nm). Inserting the nucleotides between lamellae is observed to significantly enhance the smectic ordering, with the appearance of third and fourth lamellar orders as well as a narrowing of all the previously observed peaks.

on top of what appears to be rather close to a form factor *minimum* associated to the fourth lamellar order. This difference between the form factors may be associated to changes introduced by the anionic behavior of DNA into the electron density profile of the system [41]. In addition, as discussed before, the diffuse signal between the second and third lamellar orders for the DNA-containing system arises from correlations between nucleotides.

These findings show that DNA addition induces a type of “hardening” in the system, increasing the number of correlated layers and decreasing the amplitude of fluctuations. In order to tentatively explain such effect, we wish to present two conjectures. In the first one, direct interactions between adjacent membrane surfaces would be mediated by the inserted particles. The soft nature of the forces involved in the stabilization of the lamellae (van der Waals attractions, hydration and undulation repulsions) would then be somewhat modified by DNA-membrane ion-dipole (attractive) interactions [28,29] which would act as “cement” of the complex. In the second conjecture, the rods between bilayers would restrict the space available for membrane fluctuations, resulting in an enhanced purely steric repulsion, as has been observed in lamellar phases hosting (spherical) colloidal particles [42–44]. Such a restriction would decrease disorder, allowing a growth in the number of correlated layers. Moreover, this latter mechanism could be also related to the formation of organized DNA lattices. Indeed, in other studies in the literature, the appearance of ordered structures embedded in mul-

tilamellar phases seems to be closely associated to the reduction of fluctuations. In refs. [6] and [12], centered-rectangular phases appear associated to $L_\alpha \rightarrow L_\beta$ transitions. In ref. [13] a simple rectangular structure emerged by varying the temperature and, in ref. [33], columnar hexagonal phases were obtained from steric confinement. In all these cases, a common feature is the reduction of membrane fluctuations in such a way that the latter, associated to packing constraints, could be a general agent driving the phase behavior.

The above-suggested conjectures obviously have a speculative character and the understanding of the detailed mechanisms involved in complexation and phase behavior of lipids-DNA systems remains elusive to date, especially for highly ordered domains. In spite of the minor role played by electrostatics on DNA-membrane interactions, one cannot neglect the electric interplay between DNA molecules themselves. A full understanding of the processes described here requires high-quality data about both electrostatic (ion-ion, but also ion-dipole) and steric forces. Investigations are in progress in our group, modulating the ionic strength and therefore ion-ion interactions in the system, and altering membrane flexibility and composition.

4 Conclusions

We have demonstrated a rich polymorphism of DNA superlattices embedded in multilamellar phases of lipids. The complexes studied here were prepared using zwitterionic lecithin and non-ionic fatty acid derivatives as host phase. No additional ions were used in order to mediate the complexation. Despite the absence of strong (ion-ion) electrostatic interactions between particles and membranes, we have observed a full incorporation of nucleotides to the lipid phase. The formation of single phase domains was found to be strongly dependent on the amount of DNA, suggesting a major role of packing constraints and short-range forces in complexation. Confinement was found to have dramatic effects on the supramolecular assembly of the complex. As a function of hydration, from weak DNA-DNA in-plane correlations to highly ordered columnar rectangular and hexagonal structures are found. The simple geometric models proposed here seem to be a fitting way to describe such organizations, especially when the separation between membranes is large enough to accommodate DNA rods without need for deformations of bilayers.

The addition of nucleic acids appears to improve the smectic ordering of the host phase and a mechanism based on steric reduction of membrane fluctuations is suggested, but remains to be implemented in theoretical approaches following ref. [32]. The reduction of the space between membranes implies a decrease of the degree of freedom for fluctuations, allowing the organization of DNA into strongly correlated superstructures. Experiments are in progress in order to bring some insight into the mechanisms involved in complexation.

We are grateful to the scientific team of the SWING beamline, in particular to Dr. Javier Perez, for help and support and to SOLEIL for allocating beam time to proposal 20100052. We thank Isabelle Ly and Dr. Émilie Pouget (both at Centre de recherche Paul-Pascal) for invaluable help in preparing freeze-fracture replicas and with electron microscopy observations. Prof. Gilles Sigaud is greatly acknowledged for helpful discussions about the interpretation of FFTEM images. E.R.T.S. also thanks the French Ministry of Foreign and European Affairs for an Eiffel-doctoral fellowship. This project was supported by the CAPES-CoFÉCUB French-Brazilian program under grant n° 558/07.

References

- M. Malmsten, *Soft Matter* **2**, 760 (2006).
- R. Koynova, B. Tenchov, *Soft Matter* **5**, 3187 (2009).
- J.N. Israelachvili, *Intermolecular and Surfaces Forces* (Academic Press Limited, London, 1991) pp. 341-364.
- P.L. Felgner, *Proc. Natl. Acad. Sci. U.S.A.* **84**, 7413 (1987).
- P.L. Felgner, G.M. Ringold, *Nature* **337**, 387 (1989).
- R. Koynova, R. MacDonald, *Nanolett.* **4**, 1475 (2004).
- V.A. Rakhmanova, E.V. Pozharski, R.C. MacDonald, *J. Membr. Biol.* **200**, 35 (2004).
- C. Safinya, *Curr. Opin. Struc. Biol.* **11**, 440 (2001).
- J. Gustafsson, G. Arvidson, G. Karlsson, M. Almgren, *Biochim. Biophys. Acta* **1235**, 305 (1995).
- B. Sternberg, F.L. Sorgi, L. Huang, *FEBS Lett.* **356**, 361 (1994).
- J.O. Rädler, I. Koltover, T. Salditt, C.R. Safinya, *Science* **275**, 810 (1997).
- F. Artzner, R. Zantl, G. Rapp, J.O. Rädler, *Phys. Rev. Lett.* **81**, 5015 (1998).
- G. Caracciolo, D. Pozzi, R. Caminiti, G. Mancini, P. Luciani, H. Amenitsch, *J. Am. Chem. Soc.* **129**, 10092 (2007).
- J.J. McManus, J.O. Rädler, K.A. Dawson, *Langmuir* **19**, 9630 (2003).
- J.J. McManus, J.O. Rädler, K.A. Dawson, *J. Am. Chem. Soc.* **126**, 15966 (2004).
- I. Koltover, T. Salditt, J.O. Rädler, C.R. Safinya, *Science* **281**, 78 (1998).
- H. Liang, D. Harries, G.C.L. Wong, *Proc. Natl. Acad. Sci. U.S.A.* **102**, 11173 (2005).
- K.K. Ewert, H.M. Evans, A. Zidovska, N.F. Boussein, A. Ahmad, C.R. Safinya, *J. Am. Chem. Soc.* **128**, 3998 (2006).
- A. Bilalov, U. Olsson, B. Lindman, *Soft Matter* **7**, 730 (2011).
- D. Harries, S. May, W.M. Gelbart, A. Ben-Shaul, *Biophys. J.* **75**, 159 (1998).
- S. May, D. Harries, A. Ben-Shaul, *Biophys. J.* **78**, 1681 (2000).
- O. Farago, N. Grønbech-Jensen, P. Pincus, *Phys. Rev. Lett.* **96**, 018102 (2006).
- O. Farago, N. Grønbech-Jensen, *J. Am. Chem. Soc.* **131**, 2875 (2009).
- O. Farago, N. Grønbech-Jensen, *Soft Matter* **7**, 4302 (2011).
- L. Golubović, M. Golubović, *Phys. Rev. Lett.* **80**, 4341 (1998).
- C.S. O'Hern, T.C. Lubensky, *Phys. Rev. Lett.* **80**, 4345 (1998).
- J.J. McManus, J.O. Rädler, K.A. Dawson, *J. Phys. Chem. B* **107**, 9869 (2003).
- R.J. Clarke, C. Lüpfer, *Biophys. J.* **76**, 2614 (1999).
- W. Hu, P.R. Haddad, K. Hasebe, M. Mori, K. Tanaka, M. Ohno, N. Kamo, *Biophys. J.* **83**, 3351 (2002).
- T. Pott, D. Roux, *FEBS Lett.* **511**, 150 (2002).
- D. Roux, P. Chenevier, T. Pott, L. Navailles, O. Regev, O. Mondain-Monval, *Curr. Med. Chem.* **11**, 169 (2004).
- A. Colin, D. Roux, *Eur. Phys. J. E* **8**, 499 (2002).
- E. Andreoli de Oliveira, E.R. Teixeira da Silva, A. Février, É. Grelet, F. Nallet, L. Navailles, *EPL* **91**, 28001 (2010).
- N.J. Servers, *Nat. Protoc.* **2**, 547 (2007).
- T. Salditt, I. Koltover, J.O. Rädler, C.R. Safinya, *Phys. Rev. Lett.* **79**, 2582 (1997).
- T. Pott, A. Colin, L. Navailles, D. Roux, *Interface Sci.* **11**, 249 (2003).
- F. Livolant, *Physica A* **176**, 117 (1991).
- A. Leforestier, F. Livolant, *Biophys. J.* **73**, 1771 (1997).
- F. Livolant, A.-M. Levelut, J. Doucet, J.-P. Benoit, *Nature* **339**, 724 (1989).
- D. Durant, J. Doucet, F. Livolant, *J. Phys. II* **2**, 1769 (1992).
- F. Nallet, R. Laversanne, D. Roux, *J. Phys. II* **3**, 487 (1993).
- V. Ponsinet, P. Fabre, *J. Phys. II* **6**, 955 (1996).
- Y. Suganuma, M. Imai, K. Nakaya, *J. Appl. Crystallogr.* **40**, S303 (2007).
- J.P. de Silva, A.S. Poulos, B. Pansu, P. Davidson, B. Kasmi, D. Petermann, S. Asnacios, F. Meneau, M. Impéror, *Eur. Phys. J. E* **34**, 4 (2011).